Cationic Porphyrin-Graphene Oxide Hybrid: Donor-Acceptor Composite for Efficient Photoinduced Electron Transfer

Larowska, D.; Lindner, A. A.; Mazurkiewicz-Pawlicka, M.; Malolepszy, A.; Stobiński, L.; Marciniak, B.; Lewandowska-Andralojc, A.;

Originally published:

March 2019

ChemPhysChem 20(2019), 1054

DOI: https://doi.org/10.1002/cphc.201900040

Cationic porphyrin-graphene oxide hybrid: a donor-acceptor composite for efficient photoinduced electron transfer

Daria Larowska[a], Aleksandra Wojcik[b], Marta Mazurkiewicz-Pawlicka[c], Artur Malolepszy[c], Leszek Stobiński[c], Bronislaw Marciniak[a] and Anna Lewandowska-Andralojc[a]*

Abstract: Non-covalent nanohybrids between cationic 5,10,15,20-tetra(4-trimethylammoniophenyl)porphyrin tetra(p-toluenesulfonate) (TMAP) and the graphene oxide sheets were prepared under two pH values (6.2 vs 1.8). The TMAP molecule was positively charged, regardless of whether the environment was either almost neutral or acidic. However, protonation of the imino nitrogens increased the overall charge of the porphyrin molecule from +4 to +6 ($TMAP^{4+}$ and $TMAP^{6+}$). It was found that at acidic pH, interaction of $TMAP^{6+}$ with GO was largely suppressed. On the other hand, results of FTIR, Raman spectroscopy, thermogravimetric analysis, atomic force microscopy and elemental analysis confirmed effective non-covalent functionalization of graphene oxide with cationic porphyrin at pH 6.2. The $TMAP^{4+}$-GO hybrids exhibited well defined structure with a monolayer of $TMAP^{4+}$ on the GO sheets as confirmed by AFM. Formation of the ground-state $TMAP^{4+}$-GO complex in solution was monitored by the red-shift of the porphyrin Soret absorption band. This ground state interaction between $TMAP^{4+}$ and GO was responsible for the static quenching of the porphyrin emission. Fluorescence was not detected for the nanohybrid which indicated that a very fast deactivation process had to take place. Ultrafast time-resolved transient absorption spectroscopy clearly demonstrated the occurrence of electron transfer from the photoexcited $TMAP^{4+}$ singlet state to GO sheets, as proven by the formation of a porphyrin radical cation.

Introduction

Graphene owing to its unique properties has attracted remarkable attention in the last decade.[1] Its band structure makes graphene display amazingly high conductivity and electron mobility. Considering the superior conductivity of graphene, using it as an electron acceptor and transporter provides an ideal way to design new dye-sensitized photocatalysts. However, graphene sheets are hydrophobic and tend to aggregate due to π-π interactions, that limit its application. On the other hand, graphene oxide (GO) sheets are hydrophilic and have tunable properties and can be applied in photocatalytic systems.[2] Graphene oxide is typically produced by chemical exfoliation of graphite through strong oxidization and is widely considered as an individual sheet of graphene decorated with various oxygen-containing functional groups (such as hydroxyl, epoxy, and carboxyl).[3] As such, GO is a promising precursor for the efficient synthesis of graphene-based nanomaterials. Non-covalent chemical modification of graphene oxide with dyes is based on molecular interactions, such as electrostatic attraction, π−π stacking and hydrogen bonding between graphene and organic molecules. The great advantage of the non-covalent functionalization strategy is that it can combine the unique properties of the chromophore and graphene, without affecting the physical properties of either moiety.[4] In addition, the synthesis is facile i.e. it requires only mixing of the dye solution with a dispersion of graphene oxide.

Among a variety of organic dyes, porphyrins are well known for their excellent photoactive properties.[5] Efficient charge transfer in the porphyrins and fullerenes or carbon nanotubes systems has been examined in details.[6]. With the discovery of graphene oxide, the functionalization graphene oxide with porphyrin has become attractive strategy to enhance efficient charge separation and transport in photocatalytic H_2 production systems.[7] To date, a few graphene-based materials derived from cationic porphyrins have been reported.[7a-d, 7g-i, 7m, 8] Wojcik et al. proved that positively charged porphyrin (5,10,15,20-tetra(1-methyl-4-pyridino) porphyrin tetra(p-toluenesulfonate) (TMPyP) non-covalently interacts with reduced graphene oxide by electrostatic and π−π stacking interactions. The authors presented results obtained by femtosecond transient absorption and photoelectrochemical measurements that clearly indicated the occurrence of photoinduced electron transfer in TMPyP-RGO nanohybrids.[7c] It was demonstrated that the tetrakis(trimethylammoniophenyl) porphyrin TMAP-GO composites can facilitate the incorporation of iron(III) ions into the porphyrin moieties, and thus they can be used as optical probes for the detection of iron (III) ions in complicated samples.[8a] Recently Yuan and coworkers constructed a noble metal free system for photocatalytic H_2 generation, using non-covalent Zn(II)-5,10,15,20-tetrakis(4-*N*-methylpyridyl) porphyrin ZnTMPyP-RGO nanocomposite decorated with MoS_2 as the co-catalyst.[7i]

Although worldwide interest in the development of porphyrin and graphene based composite materials resulted in numerous publications, there are no comprehensive studies that would combine detailed steady-state spectroscopic and time-resolved measurements with the characterization of the morphology and structure of the graphene based hybrid materials. In many reports on graphene-based materials, the interaction of graphene with the

[a] D. Larowska, Prof. B. Marciniak, Dr. A. Lewandowska-Andralojc
Faculty of Chemistry
Adam Mickiewicz University
Umultowska 89b, Poznan, 61-614, Poland
Email: alewand@amu.edu.pl
[b] Dr. A. Wojcik
Helmholtz-Zentrum Dresden-Rossendorf,
Institute of Ion Beam Physics and Materials Research
Bautzner Landstraße 400, 01328 Dresden, Germany
[c] Dr. M. Mazurkiewicz-Pawlicka, Dr. A. Malolepszy, Dr. L. Stobinski
Faculty of Chemical and Process Engineering
Warsaw University of Technology
Warynskiego 1, 00-645 Warsaw, Poland

Supporting information for this article is given via a link at the end of the document.

dyes is marked only by fluorescence quenching of organic molecules and/or photocurrent measurements.[7e, 9] Although the observed fluorescence quenching indicates efficient interaction between porphyrin and graphene, it does not elucidate the mechanism of the quenching process: energy versus electron transfer. It is worth mentioning that the possibility of static quenching as the reason for the observed decrease in the fluorescence intensity should be taken into account. In addition the quantitative analyses of the emission data of graphene-based materials should include correction for the light absorption and scattering by the GO. It needs to be also pointed out that, for the emission comparative studies, matching absorbance at the excitation wavelength is crucial.

Herein, we describe the preparation of the non-covalent nanohybrids between water soluble cationic 5,10,15,20-tetra(4-trimethylammoniophenyl)porphyrin tetra(p-toluenesulfonate) (TMAP) and the graphene oxide sheets under two different pH values (6.2 vs 1.8). The TMAP molecule is positively charged, regardless of whether the environment is either almost neutral or acidic (Figure 1). However, protonation of the imino nitrogens (pK_a = 2.7) increases the overall charge of the porphyrin molecule from +4 to +6.

GO sheets in an aqueous dispersion at neutral pH are negatively charged, thus it is expected that cationic porphyrin derivatives can be assembled onto their surfaces through electrostatic attraction and π-π stacking interactions. On the contrary, at low pH, the carboxyl groups of GO are mostly protonated[10] so that the electrostatic interaction with the cationic porphyrin is expected to be weaker. Thus it was our interest to compare the strength of the interaction of the TMAP with GO at two different pH values. We are aware of only one report that dealt with the TMAP interaction with GO at varied pH.[8c] The authors of that paper focused on the absorption and the emission properties of $TMAP^{6+}$ and $TMAP^{4+}$ in the presence of GO. However, the data analysis was not performed in a satisfactory manner, e.g. there was no information about the excitation wavelength used in some of the emission measurements. Quantitative analysis of the emission data can reliably be performed only when the absorbance at the excitation wavelength is kept constant. Furthermore, the shape of the emission spectra at pH 7 was not in agreement with that previously reported for that porphyrin which was left without any explanation. The authors of the paper presented only a short comment on the possible difference in the interaction strength of TMAP with GO at different pH values. Therefore, it is well justified to explore more accurately the pH influence on the TMAP-GO interaction.

In our work we put special emphasis on the methodology of all the spectroscopic measurements. One has to be aware that quantitative analysis of the data derived from absorption and emission measurements of graphene based materials needs to be done with great caution. Only then reliable results can be obtained allowing direct comparison of the properties of various systems.

Results of FTIR, Raman spectroscopy, thermogravimetric analysis (TGA), atomic force microscopy (AFM) and elemental analysis confirmed successful non-covalent functionalization of graphene oxide sheets with cationic porphyrin at pH 6.2. At acidic

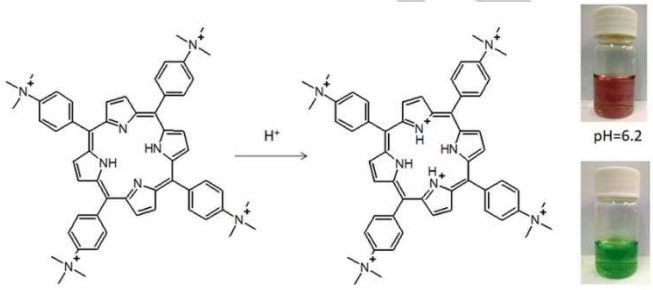

Figure 1. Structure of $TMAP^{4+}$ and $TMAP^{6+}$.

pH, interaction of $TMAP^{6+}$ with GO was largely supressed. The GO-TMAP hybrids exhibiting well defined structure, i.e. GO sheets functionalized with a monolayer of $TMAP^{4+}$, were further subjected to detailed spectroscopic characterization. We applied a number of methods to probe the ground state as well as the excited state interaction between the components of the new material. Investigations, based on steady-state and time-resolved spectroscopic measurements, indicated that at pH 6.2 a fast photoinduced electron transfer from the singlet excited state of the porphyrin to the GO moiety takes place.

It was demonstrated that introducing peripheral cationic groups allows for close contact between the porphyrin and GO surface and for ultrafast photoinduced electron transfer. However, the high quantum efficiency of electron transfer competed with undesirable charge recombination. Thus it is necessary to tune porphyrin properties by introducing other meso functional groups or metal atom in the porphyrin macrocycle to maximize the efficiency of charge separation. Only those optimized systems will constitute a promising system for artificial-photosynthesis-based device applications. Our comprehensive spectroscopic studies can provide invaluable information that can serve as guidance for fabrication other more efficient systems.

Results and Discussion

Preparation and Characterization of the TMAP−GO Hybrid Nanocomposite

As described in detail in the Experimental section, the $TMAP^{4+}$ aqueous solution was mixed with a dark brown aqueous suspension of GO, yielding a light brown suspension subjected further to centrifugation (Scheme 1). **Scheme 1**. Schematic overview of the TMAP−GO nanohybrid formation.

Figure 2 Figure 2A shows the UV-vis spectra of the suspension before and after centrifuging. It is clear that ca. 80% of the nanohybrid was successfully collected as a precipitate. An analogues experiment was performed under acidic conditions (pH

1.8), where a weaker interaction between $TMAP^{6+}$ and GO sheets was expected. The supernatant at pH 1.8 contained most of the dye used for the preparation of the nanohybrid, indicating the precipitation of GO with only small amount of the porphyrin adsorbed on it (Fig. 2B). This indicates that the formation of the nanohybrids was largely suppressed under acidic pH.

Scheme 1. Schematic overview of the TMAP—GO nanohybrid formation.

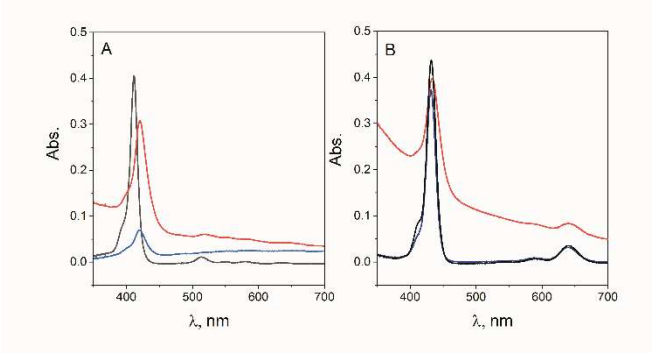

Figure 2. Absorption spectra of A) aqueous solutions (pH 6.2) of free $TMAP^{4+}$ (black), $TMAP^{4+}$ with the addition of GO suspension (red line) and spectrum of the supernatant after centrifuging (blue line), B) aqueous solutions (pH 1.8) of free $TMAP^{6+}$ (black), $TMAP^{6+}$ with the addition of GO suspension (red line) and spectrum of the supernatant after centrifuging (blue line).

The evidence for the successful functionalization of GO with porphyrin at pH 6.2 comes also from thermogravimetric analysis. Fig. 3 displays the TGA curves of GO, TMAP and TMAP-GO which were registered in argon atmosphere from room temperature to 900 °C. The mass loss of about 12% from room temperature to 115 °C for GO can be ascribed to the desorption of physically-adsorbed water on the surface and between the GO layers. The relatively large weight loss (approx. 24%) was observed around 215 °C, which is attributed to the pyrolysis of unstable oxygen containing functional groups. Around 550 °C another significant weight loss is observed which can be attributed to further decomposition of GO which is completed at the temperature of 875 °C.

In the case of TMAP, the initial weight loss of about 4% observed between 42 and 114 °C is attributed to the loss of water. In the range of 160-290 °C, up to 7.3% of the mass is lost presumably due to the partial removal of the $–N(CH_3)_3^+$ groups. The organic moiety decomposes continuously with the increasing temperature up to 1200 °C with the residue weight of 34.4%. The TGA curve of the TMAP-GO shows different behavior than the TGA curves of the free components (GO and TMAP) which indicates that the nanohybrid is a new material with its unique properties.

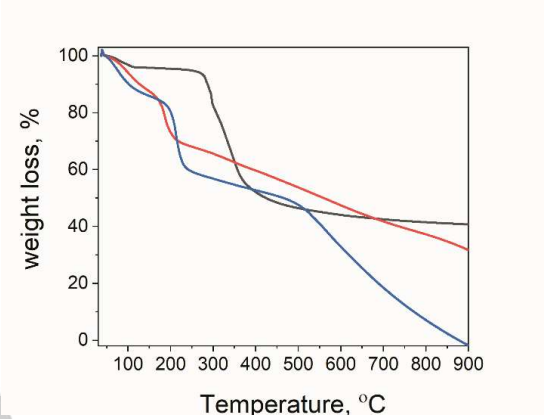

Figure 3. The thermogravimetric analysis (TGA) curves of the GO (blue), TMAP (black) and TMAP-GO nanohybrid (red).

In more detail, the step attributed to the decomposition of the oxygenated groups of GO is shifted toward lower temperatures. The characteristic peak observed in the TGA of TMAP attributed to the decomposition of the cationic moiety, is not observed in the TGA of the TMAP-GO. Electrostatic interaction of the negatively charged GO surface with the cationic groups of TMAP could increase the stability of the latter. Interestingly, the thermogravimetric analysis of the complex TMAP-GO shows that the nanohybrid is more stable than non-functionalized GO.

The FTIR spectra of the TMAP, GO and their hybrid are depicted in Fig. 4.). The spectrum of GO shows a lot of functional groups present in the structure (Fig. 4). The broad peak around 3000 cm^{-1} can be assigned to the stretching vibrations of the O-H bonds. Other notable peaks can be found at: 1719 cm^{-1} (stretching vibrations of the C=O bonds in carboxylic and carbonyl groups), 1590 cm^{-1} (skeletal vibrations of the C=C bonds in graphitic structures overlapped with the vibrations of the O-H bonds in the water molecules present in the GO sample), 1225 cm^{-1} (stretching vibrations of the C-O bonds) and 1040 cm^{-1} (stretching vibrations of the C-O-C bonds in the epoxy groups).

The FTIR spectrum of $TMAP^{4+}$ is in an agreement with its chemical structure. The absorption bands at 3410 and 967 cm^{-1} are attributed to stretching and bending vibrations of N-H and C-N, respectively, which are the characteristic absorptions of the porphyrin free base. Other notable peaks can be found at 846 and 801 cm^{-1} which are related to out-of-plane deformation of the macrocycle ring. The bands at 1010 cm^{-1}, 1118 cm^{-1} and 1175 cm^{-1} can be assigned to $C\text{-}H_{phenyl}$ vibrations. The bands at 3036 and 1475 cm^{-1} are attributed to stretching and bending vibrations of $(C\text{-}H)_{methyl}$, respectively.

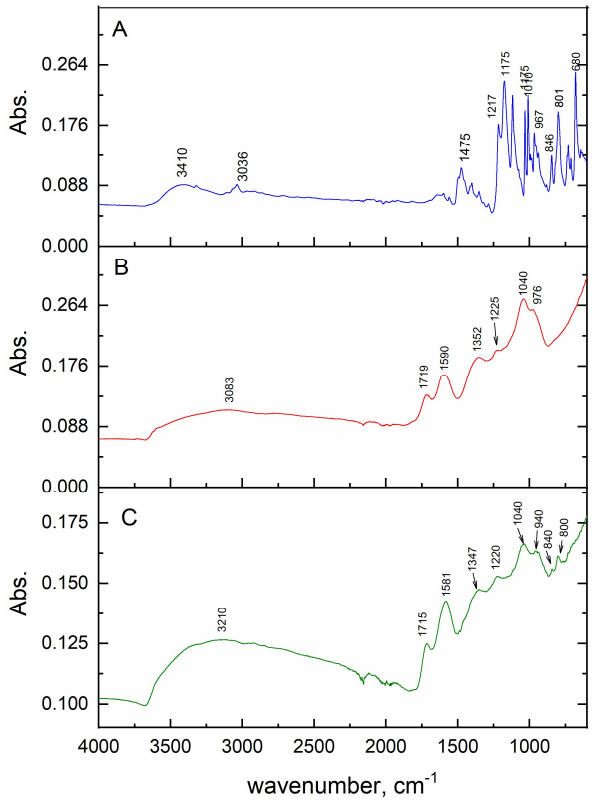

Figure 4. The FTIR spectra of the A) TMAP, B) GO and C) the TMAP-GO nanohybrid.

The FTIR spectrum of the TMAP-GO nanohybrid exhibits signals typical for the graphene oxide together with the peaks for the fingerprint region of the porphyrin, among others at 800 cm^{-1} and 840 cm^{-1}, which were not observed in the spectrum of the GO itself. Other peaks present in the nanohybrid spectrum are slightly shifted compared to GO. All these clearly confirm that the porphyrin was adsorbed on the GO surface. Adsorption of the $TMAP^{4+}$ molecules to the graphene oxide sheets was further confirmed by elemental analysis (Table 1). The sample contains low level of sulfur (<0.2%), which is the residue after the Hummers' synthesis. It has been shown in the literature even after extensive washing, the GO tends to have detectable amounts of sulfur.[11] The increased content of nitrogen in the hybrids compared to GO can be attributed to the presence of the porphyrin. Based on the increase of the carbon and hydrogen amount in the TMAP-GO, it was estimated that the prepared material contains 18% of TMAP.

Table 1. The elemental analysis results of GO and TMAP-GO.

Sample	C wt.%	H wt.%	N wt.%	S wt.%
GO	48.43	2.21	0	0.2
TMAP-GO	54.26	3.04	0.5	0.13

The effective attachment of the porphyrin molecules to the graphene oxide sheets at both protonation states of the macrocycle was further confirmed by Raman spectroscopy, as depicted on Figure 5B. In the Raman spectrum of non-functionalized graphene oxide two characteristic broad and intense peaks of comparable intensity were visible: the D band at 1348 cm^{-1} (the breathing mode of aromatic rings in the GO sheets requiring defects for its activation) and the G band at 1602 cm^{-1} (bond stretching of the sp^2 carbon pairs).[1c, 12]

In the spectra of the free $TMAP^{6+}$ and $TMAP^{4+}$ (Fig. 5A) numerous peaks were present characteristic of porphyrin derivatives.[13] The protonation state of the macrocycle only very slightly affected the peaks' spectral positions and the intensity ratios between peaks. The most intense peaks for the studied dye in both protonation states were recorded at ca. 703 cm^{-1} (out-of-plane deformation of phenyl rings), 987 cm^{-1} (out of plane deformation of C-H bonds/pyrrole breathing vibrations, peak resolvable only for $TMAP^{6+}$), ca. 1011 cm^{-1} (symmetric stretching $C_\alpha\text{-}C_m$/pyrrole breathing vibrations), ca. 1099 cm^{-1} (in-plane deformation $C_\beta\text{-}H$/ in-plane deformation C-H at phenyl rings), 1244 cm^{-1} (in-plane deformation C_m-phenyl), 1319 cm^{-1} (symmetric stretching C_α-N/asymmetric stretching $C_\alpha\text{-}C_\beta$ and in-plane deformation C_β-H), ca. 1476 cm^{-1} (asymmetric stretching $C_\alpha\text{-}C_\beta$/stretching $C_\beta\text{-}C_\beta$) and 1546 cm^{-1} (symmetric stretching $C_\beta\text{-}C_\beta$ and C_β-H/stretching $C_\beta\text{-}C_\beta$ and $C_\alpha\text{-}C_m$). Assignment of the Raman bands was carried out based on data published for similar systems.[13] The Raman spectra of both hybrids ($TMAP^{4+}$-GO and $TMAP^{6+}$-GO) confirm the attachment of the dye to graphene oxide sheets. For both nanocomposites, Raman peaks characteristic of the porphyrin macrocycle appear (compare Fig. 5A and Fig. 5B). However, signals coming from the attached dye are more pronounced for the $TMAP^{4+}$-GO pointing to a stronger interaction between the dye and the GO at neutral pH than at acidic pH. Whereas, for the $TMAP^{6+}$-GO nanocomposite, signals arising from the porphyrin molecules attached to the GO are detectable only at 1002 cm^{-1}

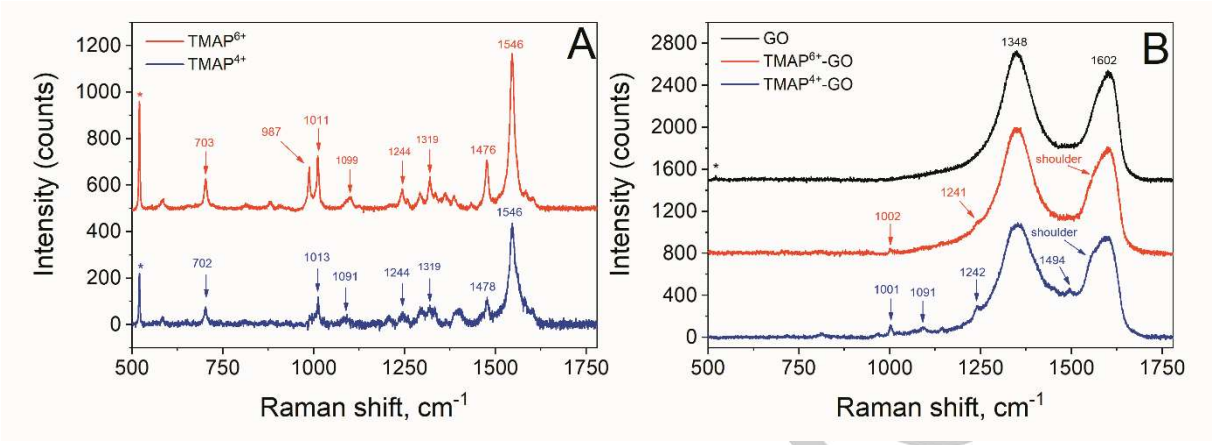

Figure 5. Raman spectra of A) the $TMAP^{6+}$ and $TMAP^{4+}$ as well as B) the GO, $TMAP^{6+}$-GO and the $TMAP^{4+}$-GO hybrids excited at 532 nm. Asterisk denotes signals coming from the substrate (Si peak at 519 cm^{-1}). Presented spectra are baseline-corrected.

and at 1241 cm^{-1}, for the $TMAP^{4+}$-GO nanocomposite not only are those two signals present, but present also are the porphyrin-related Raman peaks at 1091 cm^{-1} and at 1494 cm^{-1}. Relevant downshift (–10 cm^{-1}) or upshift (+16 cm^{-1}) of the porphyrin signal after dye immobilization on the GO sheets seem to appear only for peaks related to stretching vibrations of carbon atoms in the porphyrin macrocycle itself. This is likely indicative of the close proximity of the porphyrin core to the GO sheets. Except for the presence of the peaks characteristic of the dye, in the spectrum of the hybrids, the D band typical for the GO appeared at 1353 cm^{-1} ($TMAP^{4+}$-GO) and at 1352 cm^{-1} ($TMAP^{6+}$-GO), i.e. shifted towards higher wavenumbers as compared to non-functionalized GO by ca. 4 cm^{-1}. Additionally, the G band was registered at 1597 cm^{-1} for $TMAP^{4+}$-GO and at 1602 cm^{-1} for $TMAP^{6+}$-GO. Only for the former, was the 5 cm^{-1} downshift of the G band (as compared to the non-modified GO) indicative of effective binding of the electron-donor component to graphene oxide.[14] The D to G intensity ratio was practically identical as compared to the non-modified GO. It should also be noticed that the G band in both nanocomposites exhibited broadening towards shorter wavenumbers (referred to as a "shoulder" in Fig. 5B), arising from the overlap of the most intense porphyrin Raman peak at 1546 cm^{-1} and the G band of GO itself.

Steady state absorption

. The UV-vis spectrum of $TMAP^{4+}$ at pH 6.2 exhibited a strong Soret band centered at ca. 411 nm (ε_{411}=3.7 × 10^5 M^{-1} cm^{-1}) and four less intense Q-bands at ca. 513, 550, 587 and 633 nm. In Figure 6A are displayed the optical absorption spectra of a series $TMAP^{4+}$-GO nanohybrid suspensions, in which $TMAP^{4+}$ has a constant concentration of 1.1 μM and the concentration of GO is gradually increased. During the titration process, the intensity of the original Soret band at 411 nm decreased gradually and a new Soret band at 421 nm appeared and intensified with an isosbestic point at 416 nm. In addition, Q-band peaks shifted from 513, 550, 587, and 633 nm to 519, 554, 585 and 640 nm, respectively. By subtracting the spectrum of GO (obtained at the end of parallel titration of the blank sample (water)) from that of the $TMAP^{4+}$-GO at the end of the titration of the porphyrin solution, a spectrum of the porphyrin adsorbed on the GO surface was obtained (Fig. S1). It can be noticed that the Soret band of the $TMAP^{4+}$ adsorbed on the GO exhibits a red-shift (10 nm) and an extinction coefficient almost twice lower compared to free $TMAP^{4+}$ molecules. Only a slight broadening of the Soret band was observed for the adsorbed porphyrin. These spectral results clearly show that $TMAP^{4+}$ interacts strongly with the GO in the ground state and that the hybrids can be easily obtained by simply mixing the solutions of both components. On the basis of the spectral results described above, it is reasonable to conclude that adsorption of the $TMAP^{4+}$ on the GO sheet causes significant changes in the electronic structure of the porphyrin. The plausible explanation for the observed red shift of the Soret band in the $TMAP^{4+}$-GO is the flattening of the porphyrin structure upon adsorption on the GO sheet. Such a mechanism was proposed previously in the case of TMPyP and reduced graphene oxide (RGO) or chemically converted graphene (CCG).[7c, 7d] It is well known that the phenyl ring in the *meso*-substituted porphyrins adopts an orientation nearly perpendicular to the porphyrin plane.[15] Theoretical calculations show that only 30° twists from vertical direction can cause red-shifts of Soret bands approximately as large as 30 nm.[16]

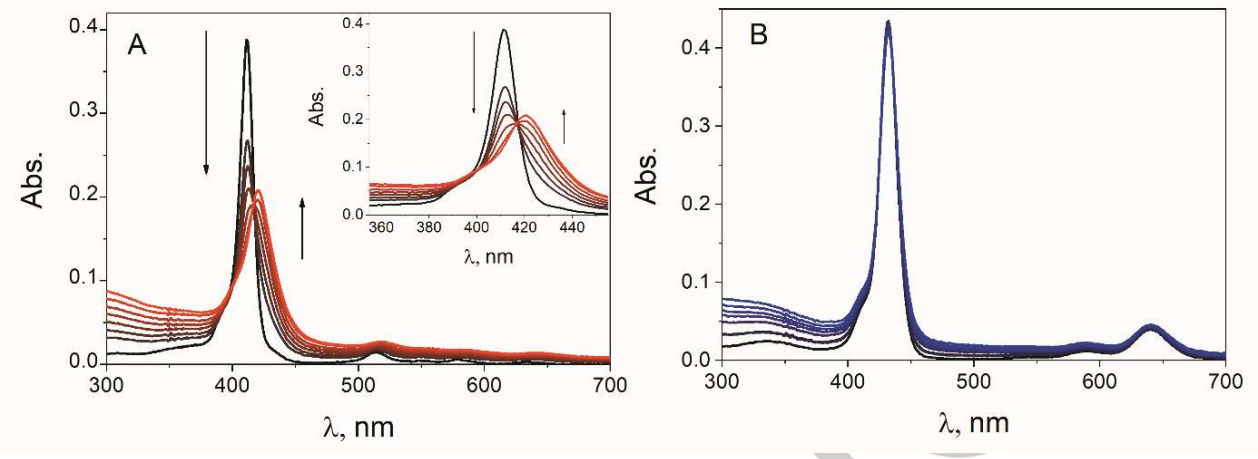

Figure 6. Absorption spectra recorded during the process of titration of 3 ml of A) 1.1 μM aqueous solution of $TMAP^{4+}$ (pH 6.2) with 0.4 mg ml^{-1} of GO dispersion (0-2.6 × 10^{-3} mg ml^{-1}). B) 1.1 μM aqueous solution of $TMAP^{6+}$(pH 1.8) with 0.4 mg ml^{-1} of GO dispersion (0-2.6 × 10^{-3} mg ml^{-1}).

The AFM images also provided solid evidence for the molecular assembly of cationic porphyrin on GO sheets. As shown in Fig. 7A, for non-functionalized GO in neutral aqueous suspension individual sheets of 0.2-3 μm lateral sizes were detected.

The GO existed as a single sheet with the apparent thickness of ca. 0.9 nm. This is in agreement with previous reports.[17] In comparison, the average thickness of a $TMAP^{4+}$-GO complex sheet (Fig. 7B) was determined to be about 1.33 nm, i.e. with 0.43 nm increment as compared with that of a pure GO sheet. It indicates successful decoration of the GO sheet with the porphyrin molecules. Considering that the thickness of one porphyrin molecule is about 0.5 nm,[18] we concluded that $TMAP^{4+}$ molecules were adsorbed on GO sheets as a monolayer, not aggregates.

Taking into account the two types of possible interactions in the nanohybrids: electrostatic attraction and π-π stacking, it is interesting to elucidate whether both of them are required for efficient adsorption of porphyrin onto GO. The role of the electrostatic interaction was studied by replacing cationic $TMAP^{4+}$ by neutral *meso*-tetra(4-pyridyl)porphyrin (TPP). The TPP structure is similar to the structure of $TMAP^{4+}$ but bears no positively charged anchoring groups on phenyl substituents. Due to lack of the solubility of the TPP in water, the measurements were carried out in methanol. No appreciable spectral changes upon titration of TPP solution with the GO suspension was observed (Fig. S2 A), although the highest GO concentration used was almost 12 times higher than the one used during titration of $TMAP^{4+}$ in aqueous solution.

Moreover, the fluorescence spectra of TPP (Fig. S3) demonstrated no decrease in the intensity upon GO addition. Based on these observations it can be stated that neutral porphyrin TPP does not interact with the GO in the ground and the excited state or that the interaction is very weak. This observation supports the hypothesis that a positive charge on the porphyrin is required to form efficiently nanoassemblies with GO by simply mixing the solutions of both components. To verify that the observed effect is not caused by the change of solvent from water to methanol, titration for the TMAP was also repeated in

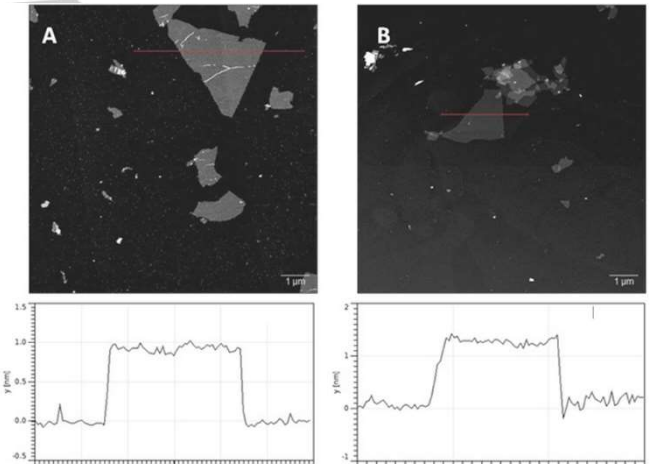

Figure 7. AFM image of A) graphene oxide, B) $TMAP^{4+}$-GO captured on mica substrate together with depth profile.

methanol (Fig. S2 B). Addition of GO resulted in a decrease of the Soret band intensity along with development of a new red-shifted Soret band at 420 nm with a similar extinction coefficient and changes of the positions of the Q-bands. The spectral changes occurring upon addition of GO were less pronounced than in water. The red shift in the position of the Soret band was only 7 nm compared to 10 nm measured in aqueous solution. In addition, a 10 times higher concentration of GO was required to achieve detectable spectral changes. Therefore, it can be concluded that the interaction between TMAP and GO in methanol is weaker than that in water but still formation of the supramolecular assembly takes place. As demonstrated by Pendolino et al., the solvent

affects the GO structure. The authors showed that the solvent does not only act as a medium for solubilizing the GO flakes but also an active interaction occurs between the graphene oxide and the molecules of the solvent.[19] Based on detailed UV-vis and FTIR analyses the authors concluded that the aromatic systems contribute more significantly to the GO structure dispersed in water than in methanol. Modification of the functional groups manifested by the further decrease of the aromatic character of the GO in methanol might be responsible for the weakening of the interaction with the porphyrin.

On the basis of the spectral results for TPP and TMAP described above, it is reasonable to conclude that the main driving force for the assembly of cationic porphyrin molecules on graphene sheets is electrostatic attraction, which is additionally facilitated by the π-π stacking cooperative interaction.

UV-vis spectra of $TMAP^{6+}$ exhibited a strong Soret Band at 431 nm (ε_{431}=3.8 × 10^5 M^{-1} cm^{-1}) with two Q-bands at 588 nm and 640 nm (Fig. 6B) The absorption spectra of $TMAP^{6+}$ was recorded with the addition of GO suspension (0 to 0.015 mg ml^{-1}) at pH 1.8 (Fig. 6B). In the presence of GO no appreciable changes in the UV-vis spectra of $TMAP^{6+}$ were registered, even though a 6 times higher concentration of GO was added as for the $TMAP^{4+}$ titration (Fig 6B). This indicates that the interaction between $TMAP^{6+}$ and GO is largely suppressed. At first a stronger interaction of $TMAP^{6+}$ with the GO compared to the $TMAP^{4+}$ might be expected due to the increase of the positive charge on the porphyrin molecules. On the other hand the pK_a of the COOH groups in GO was reported to be ~ 4.0, which indicates that GO sheets exist at an acidic pH mostly in the protonated form.[10] The plausible explanation for the weakening of the interaction between protonated porphyrin $TMAP^{6+}$ and GO can be related to the weakening of the Columbic interaction due to protonation of the oxygen containing groups in GO at low pH. In addition the change of geometry and electron density of the porphyrin after double protonation might also play a role. Theoretical calculations for various *meso*-substituted porphyrins revealed that while the porphine plane is flat in a neutral system, it is twisted to a saddle shape after double protonation, principally due to repulsive interactions between the H atoms bonded to the core N atoms.[15b, 20] It was reported that doubly protonated porphyrins (tetraphenyl porphyrin, tetra(4-carboxyphenyl) porphyrin, tetra(3,5 *di*-tert-butylphenyl) porphyrin, tetra(pentafluorophenyl) porphyrin) on the porphine center yielded no complexes with the fullerenes.[20] The authors discussed several factors that could hinder formation of the complex between protonated porphyrins and fullerene. First of all, it could be attributed to the worse contact with the fullerene surface due to distortion of the porphine ring from planarity. The saddle structure of the porphine disrupts the planar π-electron conjugation, thereby weakening the π-π interaction between porphyrin and fullerene, and the distorted *meso* substituents sterically hinder the binding of the fullerene to the porphine plane.[20] In addition, in the case of doubly protonated porphyrin, the HOMO-LUMO interaction between fullerene and porphyrin hardly stabilizes the complex because the porphyrin LUMO lies significantly lower in energy than the fullerene HOMO. The same factors might be responsible for the weak interaction between $TMAP^{6+}$ and GO.

In contrast to $TMAP^{4+}$-GO, the average thickness of a $TMAP^{6+}$-GO sheet based on AFM varied between the sheets and fluctuated around 10 nm (Fig S4). The aggregation of the $TMAP^{6+}$ is highly unlikely due to strong electrostatic repulsion among positively charged porphyrin molecules. In the case of aqueous GO solutions, the colloidal stability has been attributed to the electrostatic repulsions between ionized carboxyl groups. However, at low pH, the carboxyl groups are protonated such that the GO sheets become less hydrophilic and form suspended GO aggregates.[21] Large-scale aggregation of GO sheets at pH 1 was detected by the dynamic light scattering technique.[21] MD simulations confirmed that at pH 1 the aggregates have GO/water/GO sandwich like structures. Aggregations of the GO sheets at acidic pH reduce the GO surface available for the interaction with $TMAP^{6+}$. Indeed, at much higher GO concentration we observed spectral changes upon addition of GO to $TMAP^{6+}$ solution (Fig S5). During titration of low concentration $TMAP^{6+}$ solutions with graphene oxide up to 1.2 × 10^{-2} mg ml^{-1}, red shifts of the Soret band from 431 nm to 436 nm were observed (Fig. S5) with an isosbestic point at 438 nm. In addition, the two Q-band peaks shifted from 588 and 640 nm to 593 and 645 nm. This observation is in agreement with the data reported by Wan et al..[8c] In summary, weaker interaction between $TMAP^{6+}$ and GO can be rationalized in terms of: a) a distortion of the planarity of the porphyrin macrocycle upon protonation, b) decrease of the Columbic interaction due to protonation of the carboxylic groups in GO, c) aggregation of the GO under acidic conditions that reduces the accessibility of the GO to form assemblies with cationic porphyrin.

Further comparison of the interaction of porphyrin with GO at different pH was followed using GO films cast on glass slides. A GO coated glass slide (0.02 mg cm^{-2}) was immersed into aqueous solutions containing TMAP (28 μM) at pH 6.2 or 1.8 for 20 min and rinsed with the solvent. After drying the films in the air, the absorption spectrum was measured. An increase in the absorption with a maximum around 427 nm and 440 nm at pH 6.2 and pH 1.8 respectively was observed (Fig. 8) thereby confirming the porphyrin binding to GO film. It is noted that the Soret band of the nanohybrids was shifted by 6 nm and 4 nm for $TMAP^{4+}$ and $TMAP^{6+}$ respectively, in comparison to the experiments performed in solution.[8c] It is also apparent that more porphyrin molecules are loaded onto GO film from the solutions that contained $TMAP^{4+}$ (pH 6.2). These results again confirm that interaction of $TMAP^{6+}$ with GO sheet is weaker in acidic environment.

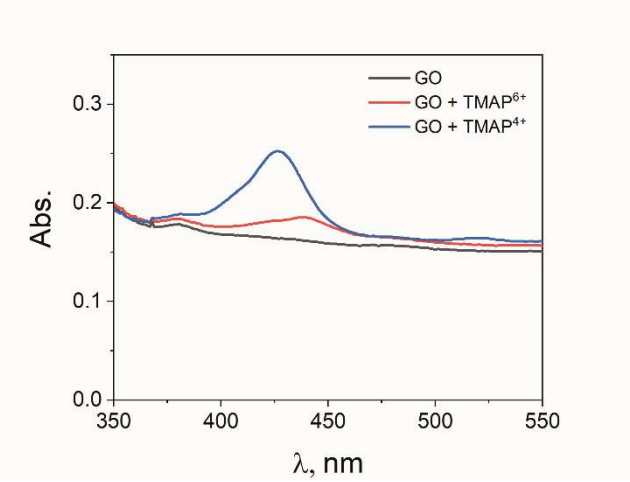

Figure 8. Adsorption of TMAP on GO film monitored by UV-vis spectroscopy. Absorption spectra of the glass slide coated with GO (black line), immersed in aqueous solutions of $TMAP^{4+}$ (pH 6.2) (blue line) and $TMAP^{6+}$ (pH 1.8) (red line) (spectra not corrected for absorption of the GO film itself).

Steady state and time-resolved emission

Photoluminescence spectroscopy was applied as a useful tool for investigation of the electronic interactions of $TMAP^{4+}$ with the GO sheets in the excited state. It should be clearly noted that quantitative analyses of the emission data of graphene-based materials are not trivial. First of all, light absorption and scattering by the GO sheets should be taken into account. Correction for the GO absorption can be done by applying the equation for inner filter effects (Eq. S1).[22] In our study the correction factor for the GO absorption at the excitation wavelength was less than 0.5%, which is related to very low concentration of GO (3.6×10^{-4} mg ml^{-1}) sufficient to quench the emission efficiently. For comparative emission studies, matching absorbance at the excitation wavelength should be used. As it was shown in the section related to absorption measurements, the absorption spectra of $TMAP^{4+}$ changes upon addition of GO. In order to keep the same absorbance at the excitation wavelength during the emission measurements, the solutions of $TMAP^{4+}$ and $TMAP^{4+}$-GO were excited at the isosbestic point i.e. 416 nm. As far as we know in none of the previous work on the interaction between TMAP and GO were the emission studies performed with excitation at the isosbestic point.[7a, 8a, 8c] A sharp decrease in the $TMAP^{4+}$ fluorescence intensity is observed with increasing GO concentration (Fig 9A).

Very often quenching of the emission intensity in the presence of the graphene type materials is considered as evidence of electron or energy transfer.[7e, 9b, 9c, 23] However, as it is discussed below, alternative mechanism of the observed decrease of the fluorescence intensity upon GO addition can operate . During the experiment two species, namely free $TMAP^{4+}$ and nanohybrid $TMAP^{4+}$-GO, are present in the solution. In general both of them could be responsible for the observed fluorescence (Scheme 2). $TMAP^{4+}$-GO has a different electronic structure as indicated by the change in its UV-vis absorption spectra in comparison to the absorption spectrum of unbound $TMAP^{4+}$. Thus it is expected that the emission of the complex would also be red shifted. However, no noticeable change in the shape/position of the peaks in the emission spectra was detected (Fig. S6). Moreover, as depicted in Fig. S7, the fluorescence excitation spectrum measured for the $TMAP^{4+}$ in the presence of GO, matches the absorption spectrum

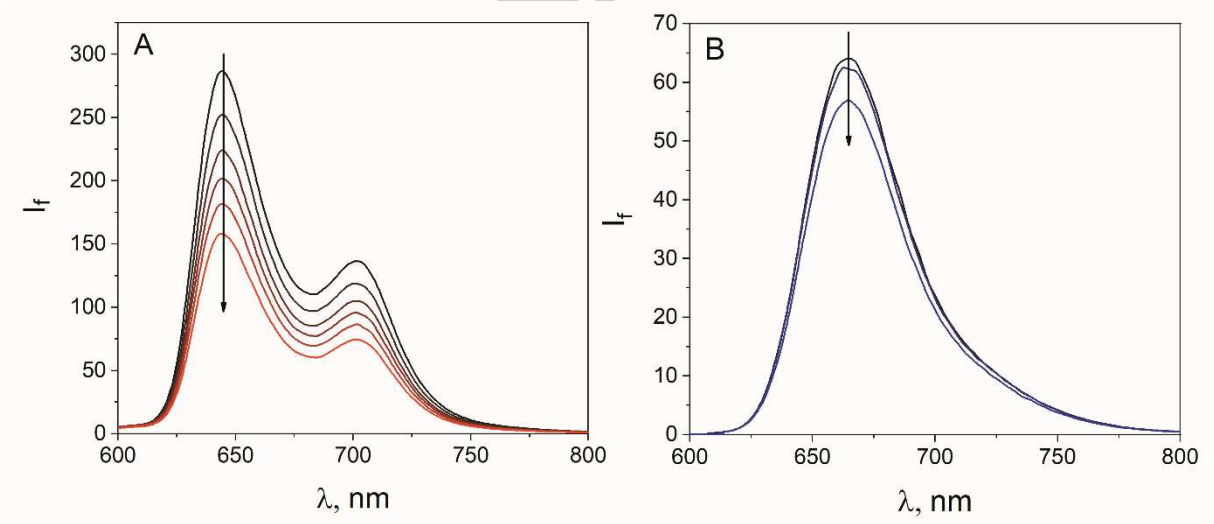

Figure 9. A) Quenching of the fluorescence of 0.3 μM $TMAP^{4+}$ in H_2O at pH 6.2 recorded during addition of an aqueous suspension of 0.08 mg ml^{-1} GO (0-3.6×10^{-4} mg ml^{-1}), λ_{exc} = 416 nm, B) Quenching of the fluorescence of 0.08 μM $TMAP^{6+}$ in H_2O at pH 1.8 recorded during addition of an aqueous suspension of 0.22 mg ml^{-1} GO (0-1.3×10^{-3} mg ml^{-1}), λ_{exc} = 438 nm.

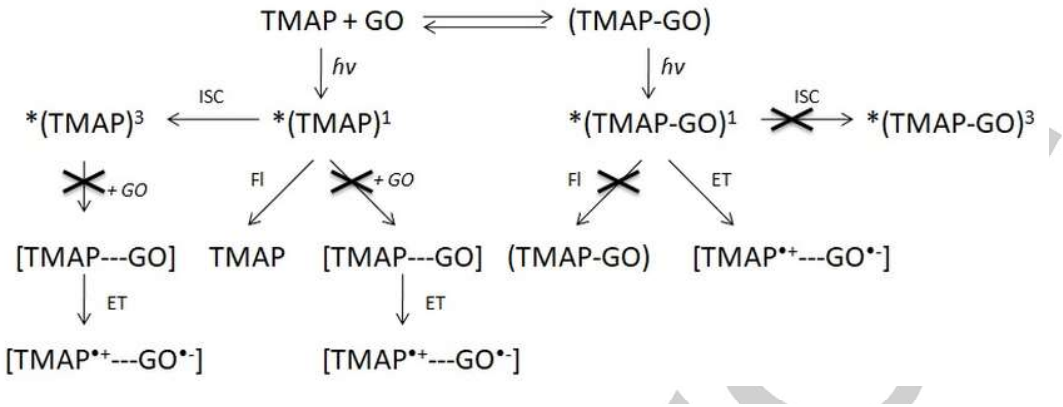

Scheme 2. Possible deactivation paths of the excited states of free TMAP and nanohybrid TMAP-GO discussed in text (FI– fluorescence, ET - electron transfer).

of free $TMAP^{4+}$. All of this data indicate that $TMAP^{4+}$ is the only emissive species present in the solution and that $TMAP^{4+}$-GO is not an emissive complex. Lack of detectable emission originating from $TMAP^{4+}$-GO suggests that the excited state of $TMAP^{4+}$-GO is deactivated very quickly. Possible explanation for the observed quenching of the fluorescence could be the interaction of the excited singlet state of the unbound $TMAP^{4+}$ with the GO i.e. dynamic quenching (Scheme 2). This possibility was examined by

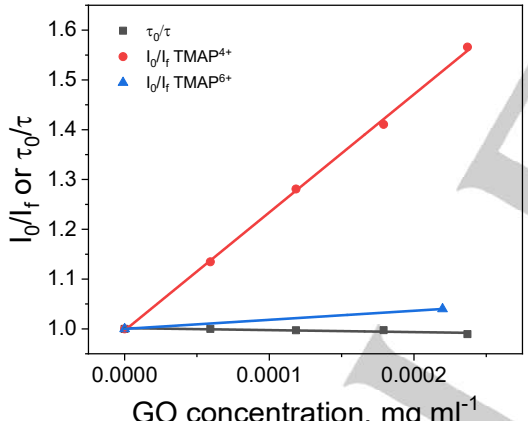

Figure 10. The relationship between fluorescence intensities I_0/I_f (I_0- fluorescence intensity without GO, I_f- fluorescence intensity after addition of GO) and GO concentration for $TMAP^{4+}$ (red) and $TMAP^{6+}$ (blue) and the relationship between fluorescence lifetimes τ_0/τ (τ_0– fluorescence lifetime without GO, τ– fluorescence lifetime after addition of GO) for $TMAP^{4+}$.

monitoring the emission decay profiles of $TMAP^{4+}$ in the presence of different GO concentrations. The fluorescence lifetime calculated from the emission decay in the absence of GO was equal to 9.8 ns. With increasing concentration of GO, no change in the decay kinetics of the excited state was observed (Fig. S8). In Fig. 10 comparison of the data obtained from the steady state and time resolved emission measurements is displayed. Lack of observable change in the singlet excited state lifetime of free $TMAP^{4+}$ excludes dynamic quenching by GO. Taking into account all these results it can be stated that the observed decrease of the fluorescence intensity can be attributed to static quenching.[24] An equilibrium between two species: fluorescent free $TMAP^{4+}$ and non-emissive complex $TAMP^{4+}$-GO exists in the solution. With the increasing concentration of GO the equilibrium is shifted toward the non-emissive complex, and the concentration of the unbound $TMAP^{4+}$ decreases, which is manifested by decreased fluorescence intensity. It is worth emphasizing here, that for the studied system the decrease of the fluorescence intensity cannot be interpreted directly as an evidence of the electron or energy transfer. However, lack of the detectable emission of the complex $TMAP^{4+}$-GO points to the possibility of a very rapid deactivation process of the excited state such as electron or energy transfer.

Upon excitation at 438 nm in the absence of GO, $TMAP^{6+}$ (pH 1.8) exhibited a broad fluorescence band over the range of 625–800 nm, with a maximum at 665 nm. As shown in Fig. 9B we found that the successive addition of GO up to 1.3×10^{-3} mg ml^{-1} into the $TMAP^{6+}$ solution had minor effect on the emission spectra. It further confirms that the interaction between $TMAP^{6+}$ and GO is limited.

Femtosecond and Nanosecond Transient Absorption Spectroscopy

To get experimental insight into the excited state dynamics between $TMAP^{4+}$ and GO, ultrafast spectroscopy experiments were carried out on both unbound $TMAP^{4+}$ and nanohybrid $TMAP^{4+}$-GO. These measurements were performed to probe whether electron transfer processes between the photoexcited

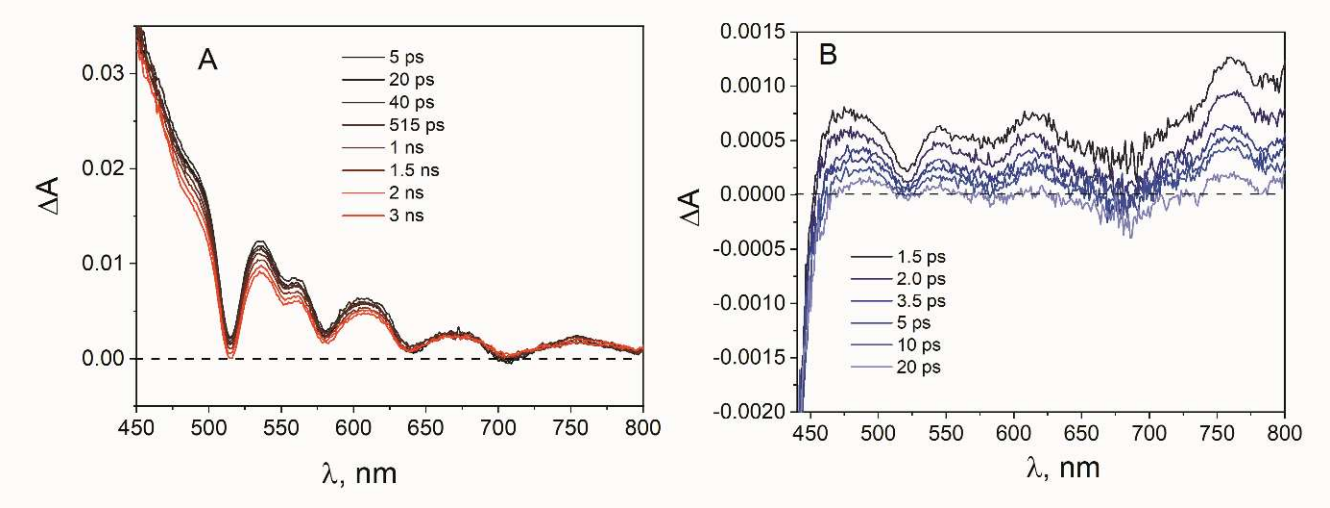

Figure 11. Transient absorption spectra registered at various time delays for A) $TMAP^{4+}$ (2.7 μM) and B) $TMAP^{4+}$-GO ($TMAP^{4+}$ concentration 0.3 μM) in water (pH 6.2) following the 420 nm laser excitation.

$TMAP^{4+}$ and graphene oxide sheets occur. The free energy of the electron transfer from the singlet excited state of $TMAP^{4+}$ to GO can be estimated by means of a Rehm–Weller type calculation.[25] The excited state energy of the porphyrin $TMAP^{4+}$ was calculated from the wavelength at the intersection point of the mutual normalized absorption/emission spectra ($E_{0\text{-}0}$ = 2.1 eV). The oxidation potential of the $TMAP^{4+}$ was taken from the literature (E_{ox} = 1.15 V vs. NHE).[26] Based on these data the oxidation potential of the singlet excited state of $TMAP^{4+}$ was calculated (E_{ox} $^{*}(TMAP^{4+})^{1}$ = –0.95 V vs NHE). Interestingly the conduction band edge of GO was found to be independent of the oxidation level and is equal to -0.55 V vs. NHE.[27] Using these values the free energy of the electron transfer from the singlet excited state of $TMAP^{4+}$ and GO was estimated to be –0.4 eV. This negative value of the free energy indicates that photoinduced electron transfer is thermodynamically allowed. Based on negligible spectral overlap between the emission of $TMAP^{4+}$ and the absorption of GO, energy transfer between the donor–acceptor components of the hybrid is highly unlikely (Fig. S9).

The spectra recorded immediately after 420 nm laser pulse excitation of $TMAP^{4+}$ at pH 6.2 show the formation of the characteristic spectrum of the singlet excited state of the porphyrin (Fig. 11A).[7a, 7c] The singlet excited state difference absorption spectra of the unbound $TMAP^{4+}$ are characterized by a broad and strong absorption around 450–500 nm and a Q-band bleach that is in agreement with the Q band position observed in the UV-vis absorption spectra. The spectra remain practically constant, undergoing only a small decay, over the whole time-window of the experiment (3 ns), in agreement with the singlet excited state lifetime measured by the TCSPC technique (9.8 ns) (Fig S10). Upon additions of GO to the $TMAP^{4+}$ solution transient absorption (TA) shows new spectral features (Fig. 11B). The lower signal to noise ratio for the TA of the nanohybrid can be related to the

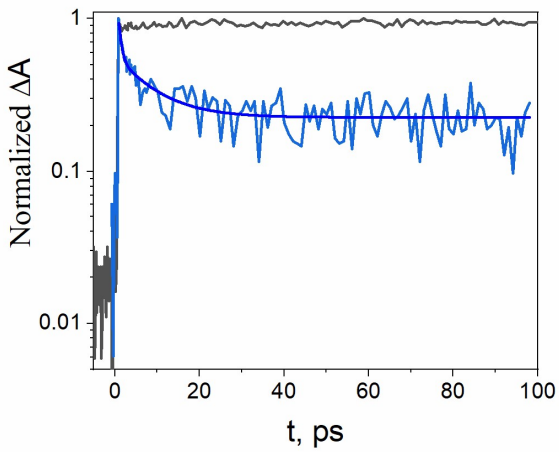

Figure 12. Transient absorption decays at 755 nm in water (pH 6.2) registered for the $TMAP^{4+}$ (black curve) and $TMAP^{4+}$-GO (red curve) following the 420 nm laser excitation.

presence of scattered light by GO. The TA taken immediately after the excitation differs from the TA of the singlet excited state of $TMAP^{4+}$. As shown in Fig. 11B, new bands in the range of 650-800 nm were observed. We assign them to the porphyrin cation radical based on a similarity to the reported spectra for TMPyP and TMAP radical cation.[7a, 7c] The detection of the radical cation provides unambiguous proof for photoinduced electron transfer from porphyrin to GO.

Kinetic traces collected for $TMAP^{4+}$ in the absence and presence of GO are given in Fig. 12. The decay of the transient absorption was registered at 755 nm, i.e. at wavelength where maximum absorbance of the porphyrin radical cation was observed for the

$TMAP^{4+}$-GO complex. Within the same time observation window, a significant difference can be noticed between the two investigated samples.The kinetic profile measured for the nanohybrid shows very fast decay dynamics (double exponential decay) compared with no decay of the excited state of free porphyrin on the same time scale of 100 ps. The time constants extracted from the decay of the $TMAP^{4+}$ radical cation are 0.4 ps and 12 ps. It is worth pointing out that the radical cation of $TMAP^{4+}$ was detected within the temporal resolution of the instrument (80 fs), indicating that the ET from the cationic porphyrin to GO is ultrafast. Such fast ET can be possible only when $TMAP^{4+}$and GO are in very close contact. Decay of the signal of the $TMAP^{4+}$ radical cation can be attributed to efficient back electron transfer and recovery of the ground state complex. Masih et al. reported that the ZnTMPyP radical ion and graphene carboxylate pairs recombined back to the initial state with a time constant of 20.18 ps, which is similar to the value measured in this study.[7g] Aly et al. also observed two time constants of a few to tens of picosecond for the decay of the $TMAP^{4+}$ radical cation formed in the presence of GC.[7a] The authors explained this observation by the occurrence of two types of donor-acceptor ion-pairs, with different degrees of the porphyrin flattening.[7a] No kinetics decays or growth were observed for the time window above 100 ps. The residual absorbance of about 10% appeared in all the recorded traces, and it is attributed to the absorption of the singlet excited state of free $TMAP^{4+}$ that was not absorbed onto the GO surface.

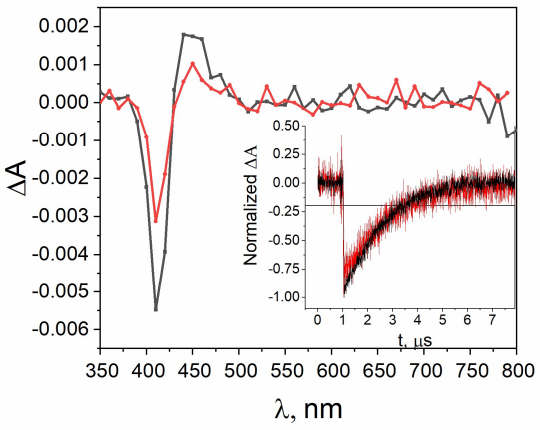

Figure 13. Transient absorption spectra obtained during laser flash photolysis (with excitation at 532 nm) of deoxygenated solutions of $TMAP^{4+}$ (black) and $TMAP^{4+}$ in the presence of GO (3×10^{-4} mg ml^{-1}) (red); time delay after flash: 100 ns. Inset: Normalized recovery profiles of the bleach monitored at 410 nm for $TMAP^{4+}$ (black) and $TMAP^{4+}$ in the presence of GO (3×10^{-4} mg ml^{-1}) (red).

To complement our studies nanosecond transient absorption measurements were conducted in order to reveal whether the interaction between $TMAP^{4+}$ and GO is also effective in the triplet state. Fig. 13 shows nanosecond transient absorption spectra registered for $TMAP^{4+}$ in the absence and presence of GO upon laser excitation at 532 nm. It should be pointed out that using 532 nm laser excitation resulted in excitation of $TMAP^{4+}$ rather than GO, due to the negligible absorbance of the latter at that particular wavelength. Upon laser excitation at 532 nm, $TMAP^{4+}$ exhibited a strong bleaching of the ground sate at 410 nm and the triplet state absorption with the maximum at 450 nm. The transient spectra exhibited no evolution during the decay of the triplet, i.e. for $TMAP^{4+}$, the triplet excited state band decayed simultaneously with the ground state bleach recovery, without any built up of new bands, indicating that the excited state of $TMAP^{4+}$ returned to its ground state (Fig. 13). Triplet lifetime was obtained from monoexponential fits of the transient decay at 450 nm and the bleach recovery at 410 nm. Both kinetic traces were characterized by the same time constant of 1.6 μs. The intensity of the transient absorption spectra decreased significantly upon addition of GO, but no spectral changes were detected (Fig. 13). No transient absorption was detected above 600 nm that would be the indication of the formation of porphyrin radical cation. At higher GO concentration the formation of the triplet state of $TMAP^{4+}$ was fully diminished. That can be explained by very fast electron transfer process from the singlet excited state which prevents intersystem crossing and as consequence suppresses the triplet state population. No change in the lifetime of the triplet state was observed upon addition of GO (Fig. 13, inset). Therefore, it can be concluded that the triplet state of the $TMAP^{4+}$ does not interact with the GO.

In summary, it was shown that there is no dynamic quenching of the singlet as well as triplet excited state of $TMAP^{4+}$ by GO (Scheme 2). The non-emissive $TMAP^{4+}$-GO complex is efficiently formed in the ground state. After excitation of the porphyrin present in the nanohybrid very fast electron transfer to GO takes place.

Conclusions

In conclusion, three points should be emphasized. First, we have demonstrated the proper methodology of conducting meaningful emission experiments in the presence of graphene type materials including the choice of excitation wavelength and correction for GO absorption. We also pointed out that it is possible to over-interpret the emission data with regard to intensity decrease being a proof of the electron transfer process between a dye and graphene. Secondly, we have proven that cationic porphyrin molecules can be efficiently assembled onto the surfaces of graphene oxide sheets forming stable complexes. During the process of assembly, it is the electrostatic attraction that plays an essential role and π-π stacking cooperative interaction can only further promote the adsorption process of porphyrin. It is shown that stronger interaction with GO occurs for $TMAP^{4+}$ than for $TMAP^{6+}$ where it is largely suppressed. This can be rationalized in terms of: a) a distortion of the planarity of the porphyrin macrocycle upon protonation, b) decrease of the Columbic interaction due to protonation of the carboxylic groups in GO, c) aggregation of the GO under acidic conditions. Thirdly, we have evidenced that the ground state interaction between $TMAP^{4+}$ and

GO causes static quenching of the porphyrin emission. Surprisingly, fluorescence is not detected for the nanohybrid which indicates that a very fast deactivation process must take place. Ultrafast time-resolved transient absorption spectroscopy clearly demonstrates the occurrence of electron transfer from the photoexcited $TMAP^{4+}$ singlet state to GO sheets, as proven by the formation of a porphyrin radical cation. However, the high quantum efficiency of electron transfer competed with undesirable charge recombination. Further studies are necessary in order to maximize the efficiency of charge separation. It can be achieved e.g. by introducing other meso functional groups or metal atom in the porphyrin macrocycle. The comprehensive wore presented here will help advance the understanding of GO interaction with porphyrin and can provide invaluable information that can serve as guidance for fabrication other more efficient systems.

Experimental Section

Materials

5,10,15,20-Tetra(4-trimethylammoniophenyl)porphyrin tetra(p-toluenesulfonate) (TMAP) and 5,10,15,20-tetra(4-pyridyl)-21*H*,23*H*-porphine (TPP) were purchased from Sigma Aldrich, graphite powder from Acros Organics. Methanol (HPLC grade) was bought from J.T. Baker. In all experiments millipore distilled water (18 MΩ cm) was used.

Preparation of the GO

Graphene oxide was prepared by oxidizing graphite powder using a modified Hummers' method.[28] Briefly, 10 g of graphite powder were mixed with 230 ml of concentrated (98 wt%) sulfuric acid at the temperature below 10 °C. Subsequently, 4.7 g of sodium nitrate and 30 g of potassium permanganate were carefully added to the mixture while the temperature was kept below 10 °C. Then the mixture was carefully heated to 30 °C and stirred for two hours. The next step involved adding 100 ml of deionized water. The slurry temperature was raised up to 100 °C. In the final step 10 ml of hydrogen peroxide were added to the mixture. The obtained dark yellow suspension was thoroughly washed and filtrated with deionized water until the pH of the filtrate reached 6.5.

Preparation of the TMAP-GO hybrid

3 ml of $TMAP^{4+}$ (1.1 μM) aqueous solution (pH 6.2) was mixed with 10 μl aqueous GO suspension (3 mg ml^{-1} GO) resulting in a light brown suspension. The mixture was centrifuged at 12000 rpm (14986 rcf) for 2 hours. The obtained supernatant was light yellow and precipitate dark brown $TMAP^{4+}$-GO powder was obtained by drying the wet precipitate in an oven for 14 h at 80 °C.

Apparatus

UV-vis absorption spectra were recorded using a two-beam spectrometer Cary 100 UV-Vis scanning from 200 to 800 nm with 1 nm increments. Quartz cells with 10 mm optical lengths were used. Fluorescence spectra were taken on a LS 50B spectrofluorometer (Perkin Elmer) with excitation and emission slits of 10 nm. Emission spectra were measured with absorbances at the excitation wavelength not higher than 0.1. Emission was scanned between 500 and 800 nm for all samples. Emission lifetimes were measured using FluoTime300 spectrometer (PicoQuant) operating in time-correlated single photon counting mode (TCSPC). A light-scattering Ludox solution (colloidal silica) was used to obtain the instrument response function (prompt). Quartz cells with 10 mm optical lengths were used for all measurements.

Femtosecond transient absorption measurements were conducted using the Solstice Ti:sapphire regenerative amplifier from Spectra Physics and an optical detection system provided by Ultrafast Systems (Helios). The source for the pump and probe pulses was the fundamental emission at 800 nm. The fundamental output was split into two beams: a pump (95%) and a probe (5%). The pump beam was directed through the TOPAS-Prime automated optical parametric amplifier from the Spectra Physics to obtain the desired excitation wavelength in the range 290-2600 nm. The probe beam was directed to the Helios: a CCD-based pump-probe TA spectrometer from the Ultrafast Systems LLC with an optical delay line allowing delays between the pump and probe up to 3.2 ns. For the detection of the transients, a white light continuum was used, which was generated from the 5% of the fundamental beam by passing it through the sapphire or calcium fluoride crystal.

The setup for the nanosecond laser flash photolysis (LFP) experiments and the data acquisition system have been previously described in detail.[29] LFP experiments employed a Nd:YAG laser (532 nm, 5 mJ, 7–9 ns) for excitation. Transient decays were recorded at individual wavelengths by the step-scan method with a step distance of 10 nm in the range of 300 to 800 nm as the mean of 10 pulses. Samples for LFP were deoxygenated with high-purity argon for 15 min prior to the measurements. Experiments were performed in rectangular quartz cells (1 cm × 1 cm). All experiments were performed with freshly prepared solutions at room temperature.

Atomic force microscopy images were recorded on an AFM Agilent 5500. The samples for the AFM measurements were prepared by dropping diluted aqueous suspensions onto a mica surface and drying in air.

Thermal properties of the samples were characterized by a thermogravimetric analyser (Mettler Toledo TGA/DSC3+). The samples' measurements were carried out under an argon atmosphere from room temperature to 900 °C at 10 °C/min. ATR-FTIR spectra were collected on a FTIR Spectrometer Nicolet iS10 (Thermo Scientific) on solid powder in the range 400-4000 cm^{-1}. Elemental analysis measurements were obtained by using a Thermo Scientific Flash 2000 CHNS/O analyzer.

Raman spectra of the samples were recorded on a LabRamHR Evolution spectrometer from Horiba Scientific coupled to a BXFM microscope (Olympus) with x100_Vis_LWD objective, using a Nd:YAG laser with a wavelength of 532 nm. Samples for Raman measurements were prepared by drop-casting a solution of $TMAP^{4+}$ or $TMAP^{6+}$ (6×10^{-5} M) and a suspension of GO (3 mg ml^{-1}) onto silicon wafers and drying in air. The nanohybrid samples for analogous measurements were prepared by drop-casting the GO suspension (3 mg ml^{-1}) on the silicon wafer, drying it in air and then immersing it in the porphyrin solution (6×10^{-5} M) for 24 h, followed by rinsing with water and drying in air.

ACKNOWLEDGMENT

This research was financially supported by the National Science Centre (project no. 2015/19/D/ST5/00682). We would like to express our gratitude to Dr. G. L. Hug for critically reading the manuscript. The authors are thankful to Dr. T. Pedzinski for his

help in femtosecond transient absorption spectroscopy measurements.

Keywords: • electron transfer •femtosecond spectroscopy • graphene oxide • nanohybrid • porphyrin

References

[1] a) D. M. Guldi, V. Sgobba, *Chem. Commun.* **2011**, *47*, 606-610; b) P. V. Kamat, *J. Phys. Chem. Lett.* **2010**, *1*, 520-527; c) C. N. R. Rao, A. K. Sood, K. S. Subrahmanyam, A. Govindaraj, *Angew. Chem. Int. Ed.* **2009**, *48*, 7752-7777; d) C. N. R. Rao, A. K. Sood, R. Voggu, K. S. Subrahmanyam, *J. Phys. Chem. Lett.* **2010**, *1*, 572-580.

[2] D. R. Dreyer, S. Park, C. W. Bielawski, R. S. Ruoff, *Chem. Soc. Rev.* **2010**, *39*, 228-240.

[3] a) S. Park, R. S. Ruoff, *Nat. Nanotechnol.* **2010**, *5*, 309; b) D. Chen, H. Feng, J. Li, *Chem. Rev.* **2012**, *112*, 6027-6053; c) S. H. Dave, C. Gong, A. W. Robertson, J. H. Warner, J. C. Grossman, *ACS Nano* **2016**, *10*, 7515-7522.

[4] V. Georgakilas, M. Otyepka, A. B. Bourlinos, V. Chandra, N. Kim, K. C. Kemp, P. Hobza, R. Zboril, K. S. Kim, *Chem. Rev.* **2012**, *112*, 6156-6214.

[5] K. Ladomenou, M. Natali, E. Iengo, G. Charalampidis, F. Scandola, A. G. Coutsolelos, *Coord. Chem. Rev.* **2015**, *304-305*, 38-54.

[6] D. M. Guldi, *Phys. Chem. Chem. Phys.* **2007**, *9*, 1400-1420.

[7] a) S. M. Aly, M. R. Parida, E. Alarousu, O. F. Mohammed, *Chem. Commun.* **2014**, *50*, 10452-10455; b) Y. Wang, Y. Zhang, J. Chen, Z. Dong, X. Chang, Y. Zhang, *Electrochemistry* **2015**, *83*, 950-955; c) A. Wojcik, P. V. Kamat, *ACS Nano* **2010**, *4*, 6697-6706; d) Y. Xu, L. Zhao, H. Bai, W. Hong, C. Li, G. Shi, *J. Am. Chem. Soc.* **2009**, *131*, 13490-13497; e) M. Zhu, Z. Li, B. Xiao, Y. Lu, Y. Du, P. Yang, X. Wang, *ACS Appl. Mater. Interfaces* **2013**, *5*, 1732-1740; f) W. Brenner, J. Malig, R. D. Costa, D. M. Guldi, N. Jux, *Adv. Mater.* **2013**, *25*, 2314-2318; g) D. Masih, S. M. Aly, A. Usman, E. Alarousu, O. F. Mohammed, *Phys. Chem. Chem. Phys.* **2015**, *17*, 9015-9019; h) T.-x. Ye, S.-l. Ye, D.-m. Chen, Q.-a. Chen, B. Qiu, X. Chen, *Spectrochim. Acta A* **2012**, *86*, 467-471; i) Y.-J. Yuan, D. Chen, J. Zhong, L.-X. Yang, J.-J. Wang, Z.-T. Yu, Z.-G. Zou, *J. Phys. Chem. C* **2017**, *121*, 24452-24462; j) D. D. La, A. Rananaware, M. Salimimarand, S. V. Bhosale, *ChemistrySelect* **2016**, *1*, 4430-4434; k) R. Ge, X. Wang, C. Zhang, S.-Z. Kang, L. Qin, G. Li, X. Li, *Colloids Surf. A* **2015**, *483*, 45-52; l) P. Guo, P. Chen, M. Liu, *ACS Appl. Mater. Interfaces* **2013**, *5*, 5336-5345; m) J. Sun, D. Meng, S. Jiang, G. Wu, S. Yan, J. Geng, Y. Huang, *J. Mater. Chem. A* **2012**, *22*, 18879-18886; n) B. Mao, D. G. Calatayud, V. Mirabello, B. J. Hodges, J. A. R. Martins, S. W. Botchway, J. M. Mitchels, S. I. Pascu, *Adv. Funct. Mater.* **2016**, *26*, 687-697.

[8] a) Z. D. Liu, H. X. Zhao, C. Z. Huang, *PLoS ONE 7* **2012**, *7*, e 50367; b) J. Geng, H.-T. Jung, *J. Phys. Chem. C* **2010**, *114*, 8227-8234; c) Y. T. Wang, X. Y. Chang, Y. Zhang, J. Q. Zhang, *J. Nanosci. Nanotechnol.* **2017**, *17*, 9027-9035.

[9] a) S. Min, G. Lu, *J. Phys. Chem. C* **2011**, *115*, 13938-13945; b) S. Min, G. Lu, *Int. J. Hydrog. Energy* **2012**, *37*, 10564-10574; c) Z. Mou, Y. Dong, S. Li, Y. Du, X. Wang, P. Yang, S. Wang, *Int. J. Hydrog. Energy* **2011**, *36*, 8885-8893.

[10] E. S. Orth, J. G. L. Ferreira, J. E. S. Fonsaca, S. F. Blaskievicz, S. H. Domingues, A. Dasgupta, M. Terrones, A. J. G. Zarbin, *J. Colloid Interface Sci.* **2016**, *467*, 239-244.

[11] A. M. Dimiev, J. M. Tour, *ACS Nano* **2014**, *8*, 3060-3068.

[12] a) G. Eda, M. Chhowalla, *Adv. Mater.* **2010**, *22*, 2392-2415; b) S. Stankovich, D. A. Dikin, R. D. Piner, K. A. Kohlhaas, A. Kleinhammes, Y. Jia, Y. Wu, S. T. Nguyen, R. S. Ruoff, *Carbon* **2007**, *45*, 1558-1565.

[13] a) J. Chen, J.-M. Hu, Z.-S. Xu, R.-S. Sheng, *Appl. Spectrosc.* **1993**, *47*, 292-295; b) H. Wang, J. Xu, J. Wan, Y. Zhao, X. Zheng, *J. Phys. Chem. B* **2010**, *114*, 3623-3632.

[14] M. Zhu, Y. Dong, B. Xiao, Y. Du, P. Yang, X. Wang, *J. Mater. Chem.* **2012**, *22*, 23773-23779.

[15] a) F. J. Vergeldt, R. B. M. Koehorst, A. van Hoek, T. J. Schaafsma, *J. Phys. Chem.* **1995**, *99*, 4397-4405; b) M. Aydin, D. L. Akins, in *Applications of Molecular Spectroscopy to Current Research in the Chemical and Biological Sciences* (Ed.: M. T. Stauffer), InTech, Rijeka, **2016**, p. Ch. 10; c) M. Aydin, *Molecules* **2014**, *19*, 20988.

[16] Z. Chernia, D. Gill, *Langmuir* **1999**, *15*, 1625-1633.

[17] H. A. Becerril, J. Mao, Z. Liu, R. M. Stoltenberg, Z. Bao, Y. Chen, *ACS Nano* **2008**, *2*, 463-470.

[18] W. Haiyan, Daxiong, H., Na, L. et al, *J. Incl. Phenom. Macrocycl. Chem.* **2005**, *52*, 247.

[19] F. Pendolino, G. Capurso, A. Maddalena, S. Lo Russo, *RSC Adv.* **2014**, *4*, 32914-32917.

[20] D.-M. Chen, X. Liu, T.-J. He, F.-C. Liu, *Chem. Phys.* **2003**, *289*, 397-407.

[21] C.-J. Shih, S. Lin, R. Sharma, M. S. Strano, D. Blankschtein, *Langmuir* **2012**, *28*, 235-241.

[22] B. Marciniak, *J. Chem. Educ.* **1986**, *63*, 998-1000.

[23] W. Zhang, Y. Li, S. Peng, *ACS Appl. Mater. Interfaces* **2016**, *8*, 15187-15195.

[24] J. R. Lakowicz, *Principles of fluorescence spectroscopy*, Springer US,, **2006**.

[25] A. Weller, *Zeitschrift für Physikalische Chemie* **1982**, *133*, 93-98.

[26] K. Kalyanasundaram, M. Neumann-Spallart, *J. Phys. Chem.* **1982**, *86*, 5163-5169.

[27] T.-F. Yeh, F.-F. Chan, C.-T. Hsieh, H. Teng, *J. Phys. Chem. C* **2011**, *115*, 22587-22597.

[28] L. Stobinski, B. Lesiak, A. Malolepszy, M. Mazurkiewicz, B. Mierzwa, J. Zemek, P. Jiricek, I. Bieloshapka, *J. Electron. Spectrosc. Relat. Phenom.* **2014**, *195*, 145-154.

[29] T. Pedzinski, Markiewicz, A. Marciniak, B. , *Res. Chem. Intermed.* **2009**, *35*, 497-506.

ARTICLE

Porphyrin-GO complex: non-covalent cationic porphyrin-graphene oxide nanohybrids: the pH dependent behaviour. Electrostatic attraction facilitates the formation of stable complex. Efficient electron transfer process occurs from the photoexcited singlet state of the porphyrin to GO.

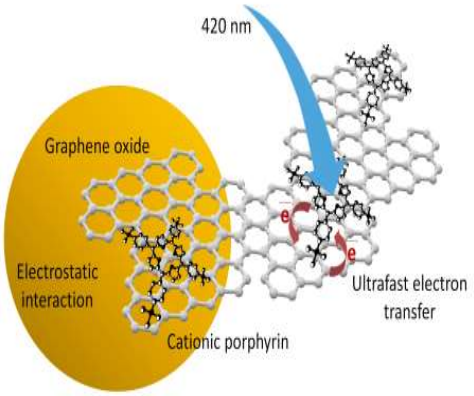

*Daria Larowska, Aleksandra Wojcik, Marta Mazurkiewicz-Pawlicka, Artur Malolepszy, Leszek Stobiński, Bronislaw Marciniak, Anna Lewandowska-Andralojc**

Page No. – Page No.

Cationic porphyrin-graphene oxide hybrid: a donor-acceptor composite for efficient photoinduced electron transfer